ELSEVIER

Journal of Power Sources 76 (1998) 69–80

JOURNAL OF POWER SOURCES

Optimal fuel cell system design considering functional performance and production costs

D. Xue [a,*], Z. Dong [b,1]

[a] Department of Mechanical and Manufacturing Engineering, University of Calgary, Calgary, Alberta, Canada T2N 1N4
[b] Department of Mechanical Engineering, University of Victoria, Victoria, British Columbia, Canada V8W 3P6

Received 19 April 1998; accepted 7 August 1998

Abstract

In this work the optimization-based, integrated concurrent design method is applied to the modelling, analysis, and design of a transportation fuel cell system. A general optimal design model considering both functional performance and production costs is first introduced. Using the Ballard Mark V Transit Bus fuel cell system as an example, the study explores the intrinsic relations among various fuel cell system performance and cost aspects to provide insights for new cost-effective designs. A joint performance and cost optimization is carried out to demonstrate this new approach. This approach breaks the traditional barrier between design (concerning functional performance) and manufacturing (concerning production costs), allowing both functional performance and production costs to be fed into design phase and to be jointly optimized.

Keywords: Concurrent engineering design; Functional performance; Production costs; Optimization; Fuel cell system

1. Introduction

A great technical challenge in our life time is to protect the environment and to clean up the messes that technology has created, especially through auto pollution. For years, a battery-powered electric car presented the main solution to a zero-emission vehicle. However, present technology cannot produce a battery that is both powerful and cheap enough as an internal combustion (IC) engine, and there is no guarantee that such a battery is even possible.

As an efficient and clean engine, fuel cell is an ideal solution for zero-emission transportation applications. A proton exchange membrane (PEM) fuel cell allows the fuel gas (hydrogen, or natural gas, or methanol, etc.) and oxygen in the air to react slowly through a semi-permeable membrane, generating DC electricity, some heat (at about 80°C), and water. The efficiently converted chemical energy is then used to drive the DC motor of an electric vehicle. The PEM fuel cells typically operate with 40–60% efficiency versus the efficiency of an IC engine of less than 35%. The fuel cells are most efficient at partial load, rather than near full load as an IC engine, providing an ideal power curve for a typical transportation load cycle. Recent research indicates that fuel cells are likely to replace IC engines in the next century [1,2].

However, application of the fuel cell technology to transportation is still in its infancy. Much research and development needs to be carried out to transfer this mature space technology to the use in our daily life. As part of these efforts, a number of researchers teamed up at the University of Victoria to develop the next generation fuel cells for transportation (NGFT), in collaboration with the international leader in transportation fuel cell technology —Ballard Power Systems Inc.

Initially developed for space applications, existing fuel cell system designs were performance-driven with modest consideration on production costs. The success of transportation fuel cell development then relies heavily on whether we can significantly reduce its production costs without considerably sacrificing the system performance. Due to the complexity of the system and the many issues

* Corresponding author. Tel.: +1-403-220-4168; Fax: +1-403-282-8406; E-mail: xue@enme.ucalgary.ca
[1] Tel.: +1-250-721-8693; Fax: +1-250-721-6051; E-mail: zdong@me.uvic.ca.

0378-7753/98/$19.00
PII: S0378-7753(98)00142-6

involved, the balance of fuel cell system functional performance and production costs is a non-trivial task.

In this work, a systematic study on the modeling, analysis, and optimization of fuel cell system functional performance and production costs is carried out. The study explores the intrinsic relations among various fuel cell system performance and cost aspects (and parameters) to provide insights for new cost-effective designs. This effort breaks the traditional barrier between design (concerning functional performance) and manufacturing (concerning production costs), allowing both functional performance and production costs to be fed into design phase and to be jointly optimized. The work is a continuation of the authors' earlier work on integrated concurrent engineering design [3–5].

2. Formulation of the optimal design considering functional performance and production cost

2.1. Design variables, functional performance and production costs

A mechanical design is specified by a large number of design parameters. Among those, several key parameters often dominate the function performance of the design and heavily influence its production costs. These parameters are identified through sensitivity study and are used as design variables, $\mathbf{d} = (d_1, d_2, \cdots, d_n)^{\mathrm{T}}$. These variables may include continuous variables, such as dimensions and tolerances, as well as discrete variables, such as part material types and surface treatment methods.

Functional performance, $F(\mathbf{d})$, is the quality measure of a design from the design aspect and a function of design variables. This measure often combines a number of individual functional performance functions, $F_i(\mathbf{d})$ $(i = 1,2, \cdots, p)$, such as power density, peak power, and dynamic response. The overall functional performance of a design is a function of all contributing functional performance measures:

$$F(\mathbf{d}) = f\big(F_1(\mathbf{d}), F_2(\mathbf{d}), \cdots, F_p(\mathbf{d})\big) \quad (1)$$

Similarly, production costs, $C(\mathbf{d})$, is the quality measure of a design from a manufacturing aspect and a function of design variables. This measure is obtained by adding all contributing costs $C_j(\mathbf{d})$ $(j = 1,2, \cdots, q)$ for producing the design:

$$C(\mathbf{d}) = \sum_{j=1}^{q} C_j(\mathbf{d}) \quad (2)$$

2.2. Existing methods for optimal design

Traditionally, optimal design of mechanical parts or systems is either aimed at the peak performance or least production costs, as shown in Table 1.

Table 1
Existing optimal design approaches

Design method	Formulated optimization problem
Functional performance	$\max_{\text{w.r.t. } \mathbf{d}} F(\mathbf{d})$
Priority design	subject to: $C(\mathbf{d}) \le C_0$
Production cost	$\min_{\text{w.r.t. } \mathbf{d}} C(\mathbf{d})$
Priority design	subject to: $F_i(\mathbf{d}) \ge F_{i0}$ $(i = 1, 2, \ldots, p)$

Functional performance priority design is applied when performance is the crucial factor of a product, such as the fuel cells for the space shuttle. Production cost priority design, on the other hand, is used for low tech, unimportant products in mass production. When the mathematical models of the objective and constraint functions are formed, an optimal design solution can be reached. In reality, design is often carried out based on the prior knowledge and experience following these two principles, rather than using the optimization, because the exact solution at the extreme condition often has no significance.

2.3. Concurrent design through joint optimization

Concurrent engineering design, or concurrent design, is a new design technique introduced in recent years to reduce product development lead times and to improve the life-cycle performance of product [6].

Different from the traditional, narrowly focused design practice, concurrent design contemporaneously incorporates considerations from all product life-cycle aspects, including design, manufacturing, assembly, maintenance, disposal, etc., into the design phase to produce better overall product life-cycle quality. The approach also reduces the number of re-designs, thereby shortening the product development lead times and reducing costs [7,8].

In the previous research, joint modeling, analysis, and optimization of the two most important life-cycle aspects of a product, i.e., functional performance and production costs, were conducted. Although carried out at the level of a mechanical part with various composing features, optimization has been found to be a very effective tool to allow multiple life-cycle performance measures to be jointly evaluated to reach an optimal design solution [3–5].

In this work, the optimization-based, integrated concurrent design method is extended to a general mechanical system—the transportation fuel cell system. A general optimal design model, considering both functional performance and production costs of a fuel cell system, is first introduced. Mathematical modeling on the functional performance and production costs of the Ballard fuel cell system is then carried out. An example of optimal fuel cell system design is used to demonstrate the approach. The optimization concurrently takes into account two functional performance aspects and production costs and searches the best values for two key design variables.

2.4. A general concurrent design model

Search of the optimal design, considering the overall product life-cycle performance, can be represented as a general optimization problem [5]:

$$\max_{\text{w.r.t.}\,\mathbf{d}} I(\mathbf{d}) = \lambda_F I^{(F)}(\mathbf{d}) - \lambda_C I^{(C)}(\mathbf{d}) + \lambda_S I^{(S)}(\mathbf{d}) - \lambda_M I^{(M)}(\mathbf{d}) + \ldots - \ldots \quad (3)$$

where $\mathbf{d}$ is a vector consisting of all design variables; λ_i $(0 \le \lambda_i \le 1)$ are factors used to weight various product life-cycle aspects according to the design intention; $I^{(F)}(\mathbf{d})$ and $I^{(S)}(\mathbf{d})$ are measures of functional performance and customer satisfaction, respectively; and $I^{(C)}(\mathbf{d})$ and $I^{(M)}(\mathbf{d})$ are measures of production and maintenance costs. These two cost terms are included as negative performance measures, or performance loss, in the formulation. The objective of the optimization is to maximize the overall life-cycle performance of the system, $I(\mathbf{d})$.

Although other issues can be incorporated in a similar manner, this research only focuses on the two most important life-cycle aspects, functional performance, $I^{(F)}(\mathbf{d})$, and production costs, $I^{(C)}(\mathbf{d})$. This leads to the formulation of the balanced performance and cost design:

$$\max_{\text{w.r.t.}\,\mathbf{d}} I(\mathbf{d}) = \lambda_F I^{(F)}(\mathbf{d}) - \lambda_C I^{(C)}(\mathbf{d}) \quad (4)$$

2.5. Functional performance and production cost indices

The balanced performance and cost design is aimed at identifying the best trade-off between the two controversial life-cycle aspects. These two measures of distinct nature must be transformed into a comparable reading. To this end, the dimensionless functional performance index, $I^{(F)}(\mathbf{d})$, and production cost index, $I^{(C)}(\mathbf{d})$, as specified by Eqs. (3) and (4), are introduced. The values of $I^{(F)}(\mathbf{d})$ and $I^{(C)}(\mathbf{d})$ are obtained by calculating the relative performance or cost changes using either an existing design or the average performance or cost value as a reference.

2.5.1. Using an existing design as reference

In practice, one can often generate a new design from an existing design through the improvement of its functional performance and reduction of its production costs. The quality of this new design can be evaluated by examining the amount of performance improvement and cost reduction from the existing design. This existing design serves as a reference. A similar approach is used to generate the performance and cost indices. The existing, or reference design, is described by a group of design variables, $\mathbf{d}_0$. Functional performance and production cost of this reference design are denoted as $F_{i_0} = F_i(\mathbf{d}_0)$ and $C_0 = C(\mathbf{d}_0)$, respectively. When the design is modified from its reference form, or the design vector $\mathbf{d}$ moves away from the reference point $\mathbf{d}_0$, the functional performance and production costs will change accordingly. The relative change of the functional performance and production cost values are used as the comparable, life-cycle performance indices, both in percentage form.

The functional performance change in the ith functional performance aspect, $I_i^{(F)}(\mathbf{d})$, and the overall functional performance change of the design, $I^{(F)}(\mathbf{d})$, can be calculated by:

$$I_i^{(F)}(\mathbf{d}) = \frac{F_i(\mathbf{d}) - F_{i_0}}{|F_{i_0}|}, \ (i = 1,2,\ldots,p) \quad (5)$$

$$I^{(F)}(\mathbf{d}) = \frac{\sum_{i=1}^{p} w_i I_i^{(F)}(\mathbf{d})}{\sum_{i=1}^{p} w_i} \quad (6)$$

where, $F_i(\mathbf{d})$ and F_{i_0} are calculated using the ith functional performance function, and $w_1, \cdots, w_p$ are weighting factors considering the relative importance of various functional performance aspects. The absolute value of F_{i_0} is used here to avoid a negative $I_i^{(F)}(\mathbf{d})$ term due to a negative functional performance reading.

Similarly, the relative change of the overall production costs, $I^{(C)}(\mathbf{d})$, can be calculated by:

$$I^{(C)}(\mathbf{d}) = \frac{C(\mathbf{d}) - C_0}{C_0} \quad (7)$$

2.5.2. Using average value as reference

For cases where no prior design exists, the previously discussed method cannot be applied. The functional performance and production cost indices are generated using the projected average performance and cost values as the references.

In design, a smaller, targeted area is often given or can be predicted for the selected design variables within the feasible design space. This area is either determined by the design problem, or assigned by a designer based on his or her design and manufacturing knowledge. Due to the high possibility that a design may fall into this area, the performance and cost values of a design in this area serve as good references. In this work, the average performance and cost values within this targeted area for design variables are used as the references to calculate the comparable performance and cost indices.

Suppose the n-dimensional targeted area for design variables, V, is defined by

$$V = \left\{\mathbf{d} | \mathbf{d} = (d_1, d_2, \ldots, d_n)^T\right\} \quad (8)$$

where $\mathbf{d}$ is a vector of design variables, the average values of functional performance and production costs can be calculated by:

$$\bar{F}_i = \frac{\int\int\ldots\int F_i(\mathbf{d})\mathrm{d}V}{\int\int\ldots\int \mathrm{d}V}, \ (i = 1,2,\ldots,p) \quad (9)$$

$$\bar{C} = \frac{\int\int\ldots\int C(\mathbf{d})\mathrm{d}V}{\int\int\ldots\int \mathrm{d}V} \quad (10)$$

The dimensionless function performance and production cost indices are then obtained by:

$$I_i^{(F)}(\mathbf{d}) = \frac{F_i(\mathbf{d}) - \overline{F}_i}{|\overline{F}_i|}, \ (i = 1,2,\ldots,p) \tag{11}$$

$$I^{(C)}(\mathbf{d}) = \frac{C(\mathbf{d}) - \overline{C}}{\overline{C}} \tag{12}$$

3. Modeling of functional performance and production costs for the fuel cell system

3.1. Ballard Mark V fuel cell system

Ballard Power Systems Inc., working with Science Applications International Corp. (SAIC), has built the world's first zero emission vehicle (ZEV) bus powered by Ballard's Mark V PEM fuel cells. This prototype transit bus was completed in March, 1993, as the first phase of the fuel cell bus program. The functional performance and production cost models introduced in this paper are based upon this fuel cell system. It should be noted that this model represents an early version of Ballard's fuel cell system and does not reflect the most recent technologies at Ballard.

In the Ballard bus, 24 Ballard PEM 5 kW fuel cell stacks are integrated into a 120 kW 'electric engine' by connecting these stacks in three 8-stack series strings. Pressurized hydrogen services as the fuel. Compressed air provides oxygen through an electrically driven automotive supercharger combined with a turbocharger. An electrically driven water pump circulates the cooling water in an air cooled radiator to remove the heat and to provide cooling to the fuel cell stack. An air-to-air heat exchanger, a number of filters, and water knockout components are also used in the system. The configuration of this fuel cell system is illustrated in Fig. 1.

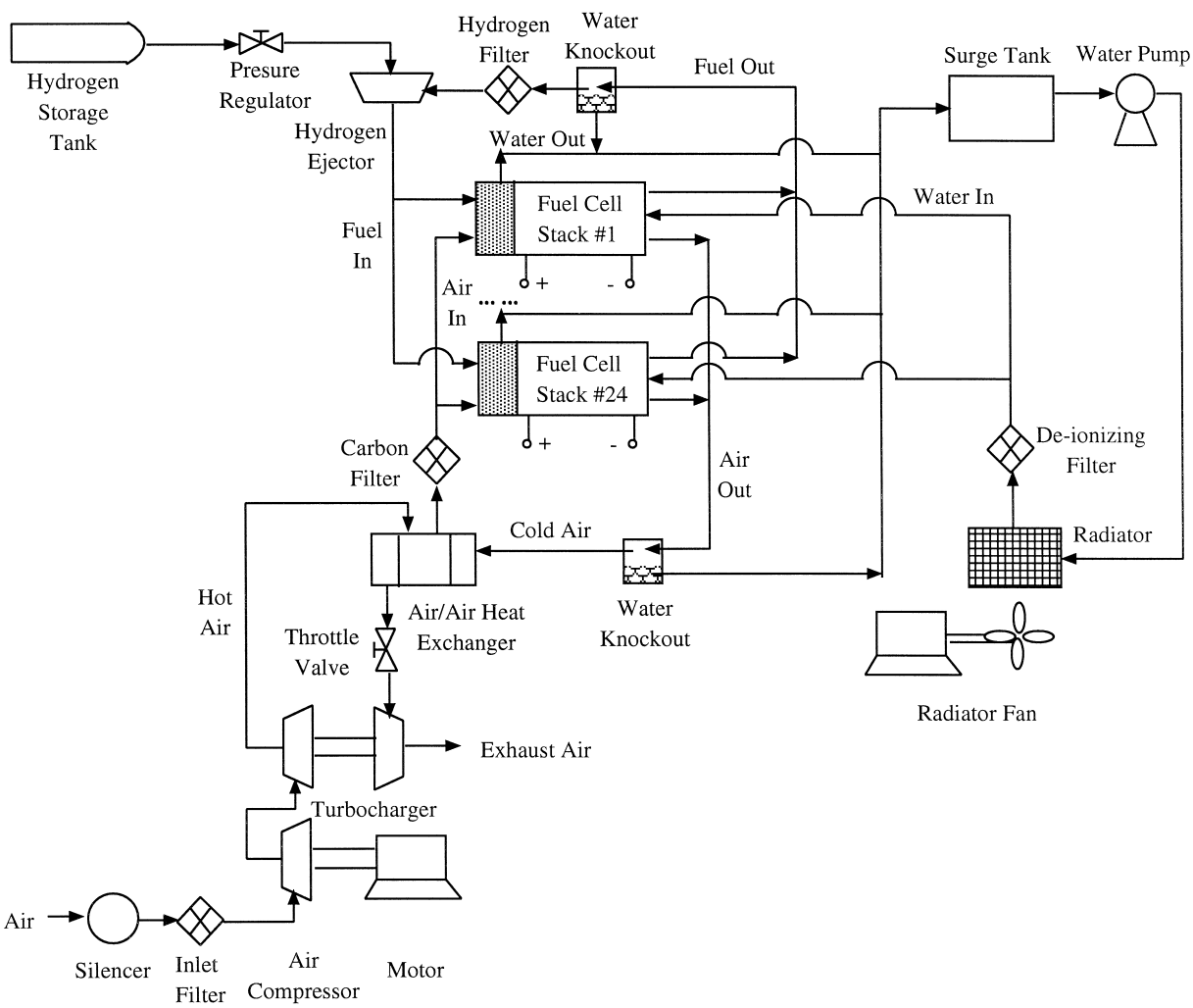

Fig. 1. Ballard fuel cell system.

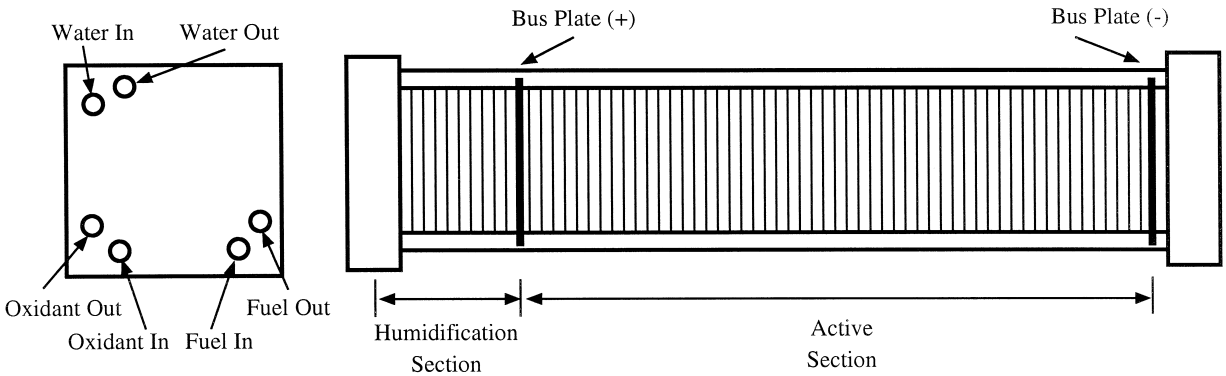

Fig. 2. A fuel cell stack.

The key components in this system are fuel cell stacks. The structure of a fuel cell stack is shown in Fig. 2. In a fuel cell stack, 35 fuel cells are connected in series. Each fuel cell consists of a membrane which is used as electrolyte, two electrodes, and two plates as shown in Fig. 3. Hydrogen fuel and air are supplied to the two electrodes through the flow channels of gas delivery plates to generate a current between the two electrodes. For each two gas delivery plates, a cooling plate is added. In addition, 10 cells for humidification are used for each stack at one end of the stack.

3.2. Design variables, functional performance, and production costs of the fuel cell system

This research focuses on the identification of the optimal design considering functional performance and production costs. The functional performance models of the Ballard fuel cells were originally developed by Amphlett et al. [9–12] and modified by Cownden and Nahon [13] considering the whole fuel cell system. The cost models of the Ballard fuel cell system were developed by Ronne and Podhorodeski [14]. The performance and cost models introduced in this work are based on the results summarized in Refs. [13,14]. Due to the complicity of the system, only a number of major design variables, performance, and cost models are considered in this work.

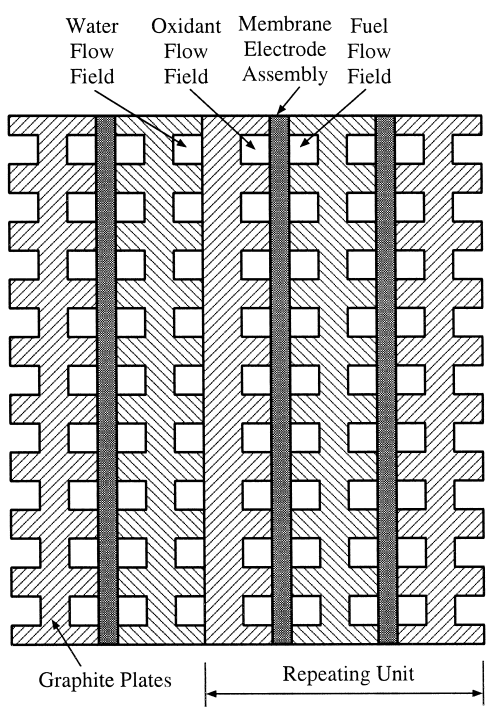

Fig. 3. Cross sections of fuel cells.

The whole system can be divided into a number of functional modules. The influence of key system parameters and design variables on functional performance and production costs is discussed based on these modules. The system parameters and design variables, as well as performance and cost measures, are only explained when they are introduced for the first time in this paper. A summary of major system parameters, design variables, performance and cost measures is listed at the end of this paper.

3.2.1. Fuel cell stack module

The reaction in a hydrogen/oxygen fuel cell can be written as [1]:

$$2H_2 + O_2 \rightarrow 2H_2O \quad (13)$$

The output voltage of the cell V_{cell}, considering thermodynamics, mass transport, kinetics, and ohmic resistance, is described by [11]:

$$V_{cell} = E + \eta_{act} + \eta_{ohmic} \quad (14)$$

where, E is open circuit output voltage; η_{act} is voltage loss due to activation; and η_{ohmic} is voltage loss due to ohmic resistance, respectively.

At present, there exists a very limited number of published PEM fuel cell performance models, even more rare for the Ballard fuel cell. In the previous work carried out by Amphlett et al., they have applied the Nernst equation [1] to calculate the open circuit output voltage that is determined by the thermodynamic potential of the reaction:

$$E = E^{\circ} - \frac{RT_k}{nF} \ln\left[p^*_{H_2} \left(p^*_{O_2} \right)^{0.5} \right] \quad (15)$$

where, E° represents a reference potential at unit activity; $p^*_{H_2}$, $p^*_{O_2}$ are effective partial pressure measures of hydrogen and oxygen; and T_k is temperature. R, n, and F are gas constant, number of equivalents involved in reaction, and Faraday's constant, respectively. This equation was used to calculate the open circuit output voltage of a Ballard Mark V PEM fuel cell [11,12]:

$$E = 1.229 - 0.85 \times 10^{-3}(T_k - 298.15) + 4.3085 \times 10^{-5} T_k \left[\ln\left(p^*_{H_2}\right) + \frac{1}{2}\ln\left(p^*_{O_2}\right) \right] \quad (16)$$

Furthermore, they used the empirical data from a Ballard Mark V fuel cell to determine a number of coefficients of the model, and come out the relations for calculating the voltage losses due to activation and ohmic resistance. Strictly speaking, these equations are not kinetic models of a fuel cell, but they provided a very good match with the measured performance of the Ballard Mark V PEM fuel cell. At present no strict kinetic models of a PEM fuel cell is available due to the complex mass transport and electrochemistry of a PEM fuel cell. This work focuses on the combined performance and cost optimization of the Ballard Mark V PEM fuel cell system, the models from Amphlett et al. allows this new approach to be implemented and demonstrated.

The voltage loss due to activation, η_{act}, is calculated by [11,12]:

$$\eta_{act} = -0.9514 + 3.12 \times 10^{-3} T_k + 7.4 \times 10^{-5} T_k \cdot \ln\left(c^*_{O_2}\right) - 1.87 \times 10^{-4} T_k \cdot \ln(I) \quad (17)$$

where, $c^*_{O_2}$ is concentration of oxygen and I is current, respectively. I is calculated using:

$$I = i \cdot A_a \quad (18)$$

where, A_a is active intersection area of the fuel cell stack; and i is current density.

The voltage loss due to ohmic resistance is calculated by [11,12]:

$$\eta_{ohmic} = -I\left(1.605 \times 10^{-2} - 3.5 \times 10^{-5} T_k + 8.0 \times 10^{-5} I\right) \quad (19)$$

The partial pressure and concentration terms used in these equations, including $p^*_{H_2}$, $p^*_{O_2}$, and $c^*_{O_2}$, can be obtained through the following procedure. First the saturation pressure of water, $p^{sat}_{H_2O}$, is calculated by [15]:

$$p^{sat}_{H_2O} = 10^{-2.1794 + 0.02953 T_c - 9.1837 \times 10^{-5} T_c^2 + 1.4454 \times 10^{-7} T_c^3} \quad (20)$$

where, T_c is the temperature in Celsius and calculated by:

$$T_c = T_k - 273.15 \quad (21)$$

The partial pressure measures $p^*_{O_2}$ and $p^*_{H_2}$ at cathode and anode are calculated by [11]:

$$p^*_{O_2} = p^{sat}_{H_2O} \cdot \left[\frac{1}{\exp\left(\frac{4.192\, i}{T^{1.334}} \right) x^{cathode}_{H_2O}} - 1 \right] \quad (22)$$

$$p^*_{H_2} = 0.5\, p^{sat}_{H_2O} \cdot \left[\frac{1}{\exp\left(\frac{1.653\, i}{T^{1.334}} \right) x^{anode}_{H_2O}} - 1 \right] \quad (23)$$

where, $x^{cathode}_{H_2O}$ and $x^{anode}_{H_2O}$ are mole fraction measures of water at cathode and anode respectively. Because $x^{cathode}_{H_2O}$ and $x^{anode}_{H_2O}$ can be calculated by:

$$x^{cathode}_{H_2O} = \frac{p^{sat}_{H_2O}}{P_{air}} \quad (24)$$

$$x^{anode}_{H_2O} = \frac{p^{sat}_{H_2O}}{P_{H_2}} \quad (25)$$

where, P_{air} and P_{H_2} are pressures of air and hydrogen respectively, Eqs. (22) and (23) can then be transformed as [10]:

$$p^*_{O_2} = \frac{P_{air}}{\exp\left(\frac{4.192\, i}{T^{1.334}} \right)} - p^{sat}_{H_2O} \quad (26)$$

$$p^*_{H_2} = 0.5 \frac{P_{H_2}}{\exp\left(\frac{1.653 i}{T^{1.334}} \right)} - p^{sat}_{H_2O} \quad (27)$$

The pressure values of air and hydrogen are usually selected as the same to keep the balance inside the fuel cell stacks.

Concentration of oxygen, $c^*_{O_2}$, is calculated by [11]:

$$c^*_{O_2} = \frac{p^*_{O_2}}{5.08 \times 10^6 \exp\left(\frac{-498}{T_k} \right)} \quad (28)$$

Power output for the fuel cell system can then be calculated by

$$W_{sys} = n_{stack} \cdot n_{cell} \cdot V_{cell} \cdot i \cdot A_a \quad (29)$$

where, n_{stack} and n_{cell} are number of stacks in the system and number of cells in a stack, respectively.

The total cost for the fuel cell stacks, C_{stacks}, is calculated by

$$C_{stacks} = n_{stacks} \cdot \left[n_{cell} \cdot C_{cell} + n_{hum} \cdot C_{hum} + C_{stk\_a} + C_{stk\_m} \right] \quad (30)$$

where, C_{cell} and C_{hum} are cost for a fuel cell and cost for a humidification cell respectively; n_{hum} is the number of humidification cells in a stack; and C_{stk_a} and C_{stk_m} are

costs for stack assembly and stack material respectively. The cost of a fuel cell is composed of the cost for Du Pont's Nafion 117™ membrane, cost for electrodes and catalyst (platinum), cost for plates including conventional plates and cooling plates, cost for membrane–electrode assembly, and so on. The cost for a humidification cell is calculated by adding the cost for the membrane and the cost for the plate. The costs for membranes, electrodes, and plates are calculated based on unit material costs and total stack intersection area A_t. The active stack intersection area, A_a, is calculated from the total stack intersection area A_t using

$$A_a = 0.56\,A_t \tag{31}$$

The cost for catalyst is a function of the active stack intersection area A_a. The machining and assembly costs are calculated based on the unit time machining costs, unit time labour costs, unit time overhead costs, and machining/assembly time measures.

3.2.2. Hydrogen supply module

The required hydrogen supply flow rate, f_{H_2}, is calculated by [9]:

$$f_{H_2} = \frac{A_a \cdot i}{n_{H_2} \cdot F} \cdot \mathrm{VSTP} \cdot n_{cell} \cdot n_{stack} \tag{32}$$

where, n_{H_2} and VSTP are electron number per hydrogen molecule and specific molar volume of gas, respectively. The actual hydrogen supply flow rate should be larger than the required hydrogen supply flow rate.

The costs of this module, C_{H_2}, include the fixed hydrogen supply system cost and fuel cost. Fuel cost is a function of actual hydrogen supply flow rate.

3.2.3. Air supply module

The required air supply flow rate, f_{air}, is calculated by:

$$f_{air} = \frac{f_{H_2}\chi}{2.0\chi_{O_2}} \tag{33}$$

where, χ_{O_2} is fraction of oxygen in the air; and χ is stoichiometric ratio of air, respectively. The stoichiometric ratio χ is selected greater than 1 to provide sufficient oxygen for reaction.

The air supply system is composed of an air compressor, a turbocharger, an air-to-air heat exchanger, a number of water knockout components, and filters. Because this research focuses on modeling the performance of the fuel cells, only a brief description is given to the supporting components in the fuel cell system.

First, the pressure drop, ΔP, through the various components including fuel cell stacks, water knockout units, filters, and heat exchanger is calculated by:

$$\Delta P = kf^2 \tag{34}$$

where, f is the flow rate; and constant, k, is the pressure drop coefficient determined by the component configuration. Using this equation, the pressure at different locations of the air supply system can be determined.

The air compressor is one of the major power consuming components in the fuel cell system. The model used to calculate the air compressor performance is based on the performance curves for an Opcon Autorator twin screw superchanger [13], which has a peak efficiency of 61%. The consumed power is a function of working pressure, temperature, air flow rate, and efficient measures of motor and air compressor. The model of the turbocharger is developed based on the performance curves for a Garrett compressor/turbine pair [13]. The compressor has a peak efficiency of 80%, while the turbine has a peak efficiency of 70%. Modeling of the heat exchanger is based on fundamental heat transfer textbooks. The temperature measures at different locations can also be obtained using these models.

The cost of the air supply system is primarily calculated by adding the costs of all composing components. Change of the fuel cell system parameters, including pressure and temperature measures in different locations and air stoichiometric ratio, will have influence on the chemical reaction in the fuel cell stacks, thereby changing the actual hydrogen supply flow rate. Therefore, these fuel cell system parameters influence the total system cost indirectly.

3.2.4. Cooling module

The cooling module is used to remove the heat generated by the reaction of hydrogen and oxygen and to humidify the incoming air and hydrogen streams. The cooling module consists of a radiator, a water pump, a radiator fan, a de-ionizing filter, and a surge tank. The radiation fan and water pump are two power consuming sources. The load of the radiator fan is a constant. The load of the water pump, according to Ref. [13], is obtained by (a) calculating the total heat which must be rejected to keep the fuel cell stacks at a constant temperature, (b) assuming that 20% of the heat is radiated by the stacks, (c)

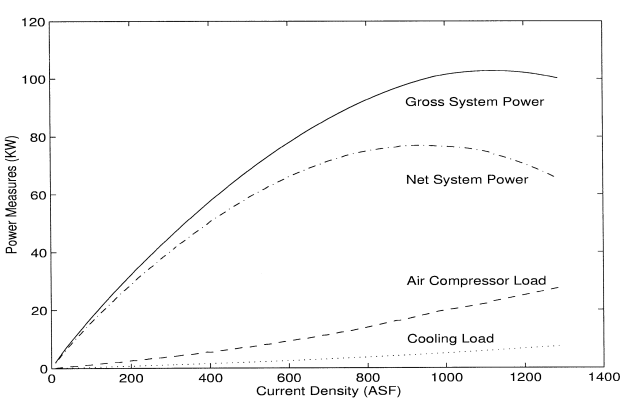

Fig. 4. Relations between current density and power measures.

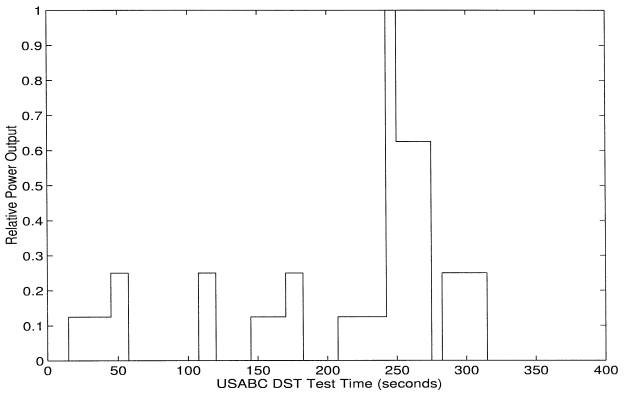

Fig. 5. USABC dynamic stress test (DST) curve.

calculating the water flow rate needed to reject the remaining 80% of the heat, and, (d) calculating the power required to drive this flow assuming the efficiencies of the pump and the motor are 50% and 70%, respectively.

The costs of the cooling module can be calculated by adding the fixed costs of all the composing components.

Based upon the models of these modules, the net system power output, W_{net}, is calculated by:

$$W_{net} = W_{sys} - W_{ac} - W_{cool} \quad (35)$$

where, W_{sys} is the gross fuel cell system power output; W_{ac} is the power consumed by the air compressor; and W_{cool} is the power consumed by the radiator fan and the water pump, respectively. Efficiency of the fuel cell system, η, is defined as:

$$\eta = \frac{W_{net}}{W_{sys}} \quad (36)$$

The total fuel cell system cost, C, is calculated by:

$$C = C_{stacks} + C_{air} + C_{H_2} + C_{cool} + C_{cont} \quad (37)$$

where, C_{stacks}, C_{air}, C_{H_2}, C_{cool}, and C_{cont} are the costs for stack module, air supply module, hydrogen supply module, cooling module, and control module, respectively.

4. Optimal design of the fuel cell system

4.1. Selection of performance and cost measures and design variables

Many system parameters influence both the functional performance and production costs of the fuel cell system. The key parameters include working pressure and temperature in the fuel cell stacks, active stack intersection area, air stoichiometric ratio, number of cells in a stack, number of stacks in the system, etc. In this work, two system parameters, the active stack intersection area, A_a, and air stoichiometric ratio, χ, are selected as design variables in the joint optimization. Two functional performance measures, the maximum net system power output, W_{net}^{max}, and the average efficiency, η_{ave}, [based upon the dynamic stress test (DST) of the United States Advanced Battery Consortium (USABC)] and the production costs of the system, C, are considered in the joint optimization.

The maximum net system power output, W_{net}^{max}, is identified based upon the relation between the current density, i, and net system power output, W_{net}. The i-W_{net} relation is shown in Fig. 4. Some other power measures, including gross system power, W_{sys}, air compressor load, W_{ac}, and cooling load, W_{cool}, are also given in Fig. 4. Current density is selected between 10 and 1300 ASF (Ampere per square feet). Default values of active stack intersection area, A_a, and air stoichiometric ratio, χ, are selected as 232.0 cm^2 and 1.75, respectively.

The USABC dynamic stress test (DST) is a method to evaluate the performance of batteries [1]. In a DST, a test cycle is divided into 16 time periods as shown in Fig. 5. Each period is associated with a relative power output value. The data used in USABC DST are summarized in Table 2, where i is the time period sequence number; t_i and ρ_i are time period length and relative power output (between 0 and 1), respectively.

By associating the maximum net power output of the fuel cell system with the maximum relative power output defined in DST, the desired net system power output at any time in the cycle can be calculated by:

$$W_{net_i} = \rho_i \cdot W_{net}^{max} \quad (38)$$

From Fig. 4, the corresponding current density can be identified, and the system efficiency η_i can be achieved using Eq. (36). The average efficiency of a DST cycle is defined as:

$$\eta_{ave} = \frac{\sum_{i=1}^{16} (\eta_i t_i)}{\sum_{i=1}^{16} (t_i)} \quad (39)$$

The calculated production costs of the fuel cell system, described by Eq. (37), is used as the measure of manufac-

Table 2
USABC dynamic stress test (DST) data

i	1	2	3	4	5	6	7	8	9	10	11	12	13	14	15	16
t_i	15.0	30.0	12.5	25.0	25.0	12.5	25.0	25.0	12.5	25.0	35.0	7.5	25.0	7.5	32.5	52.5
ρ_i	0.0	0.125	0.25	0.0	0.125	0.25	0.0	0.125	0.25	0.0	0.125	1.0	0.625	0.0	0.25	0.0

turability of the fuel cell system and is incorporated in the joint optimization. Due to proprietary limitation, only relative cost values are presented.

4.2. Evaluation of functional performance and production costs

Evaluation of functional performances, including the maximum net system power output, $W_{\text{net}}^{\max}$, and average USABC DST efficiency, η_{ave}, as well as the total production cost, C, regarding the two design variables: the active stack intersection area, A_a, and the air stoichiometric ratio, χ, is carried out using the following procedure.

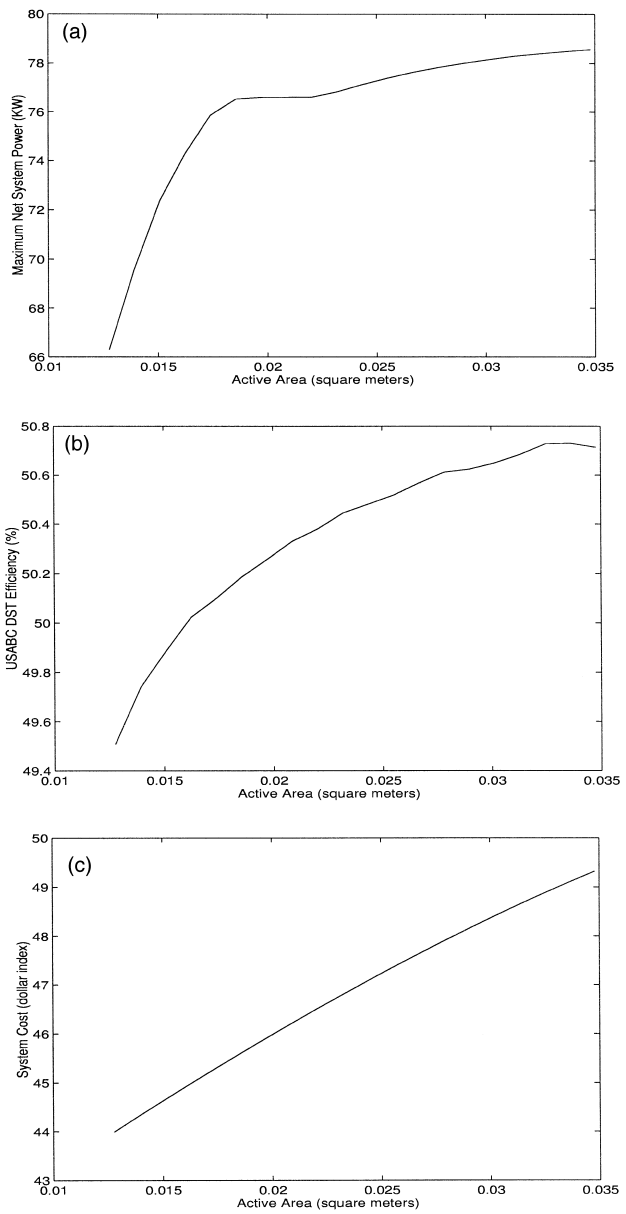

Fig. 6. Evaluation measures regarding active area. (a) Relation between active area and maximum net system power. (b) Relation between active area and USABC DST efficiency. (c) Relation between active area and system cost.

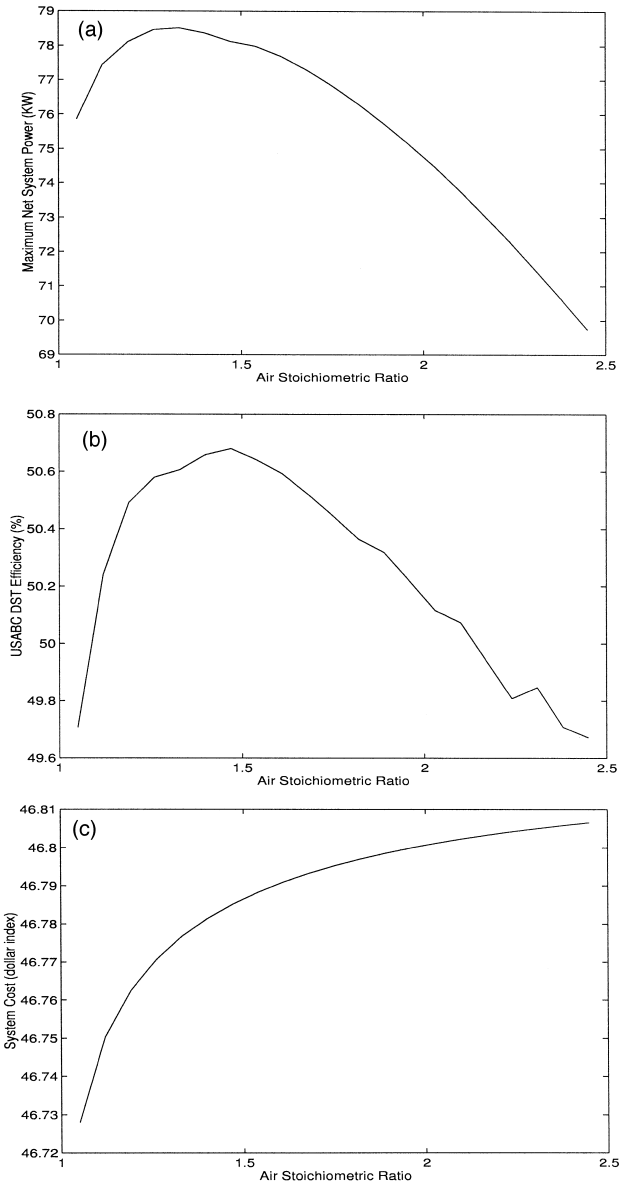

Fig. 7. Evaluation measures regarding air stoichiometric ratio. (a) Relation between air stoichiometric ratio and maximum net system power. (b) Relation between air stoichiometric ratio and USABC DST efficiency. (c) Relation between air stoichiometric ratio and system cost.

First, an analysis on the influences of the two design variables to the three performance and cost measures is carried out separately. The results are given in Figs. 6 and 7. The active stack intersection area, A_a, is changed from 1.0×10^2 m^2 to 3.5×10^{-2} m^2; and air stoichiometric ratio, χ, is changed from 1.0 to 2.5, respectively.

The results in Fig. 6 indicate that system performance and cost increase steadily with the increase of the active stack intersection area. The results in Fig. 7 illustrate poor performance readings for small and large air stoichiometric

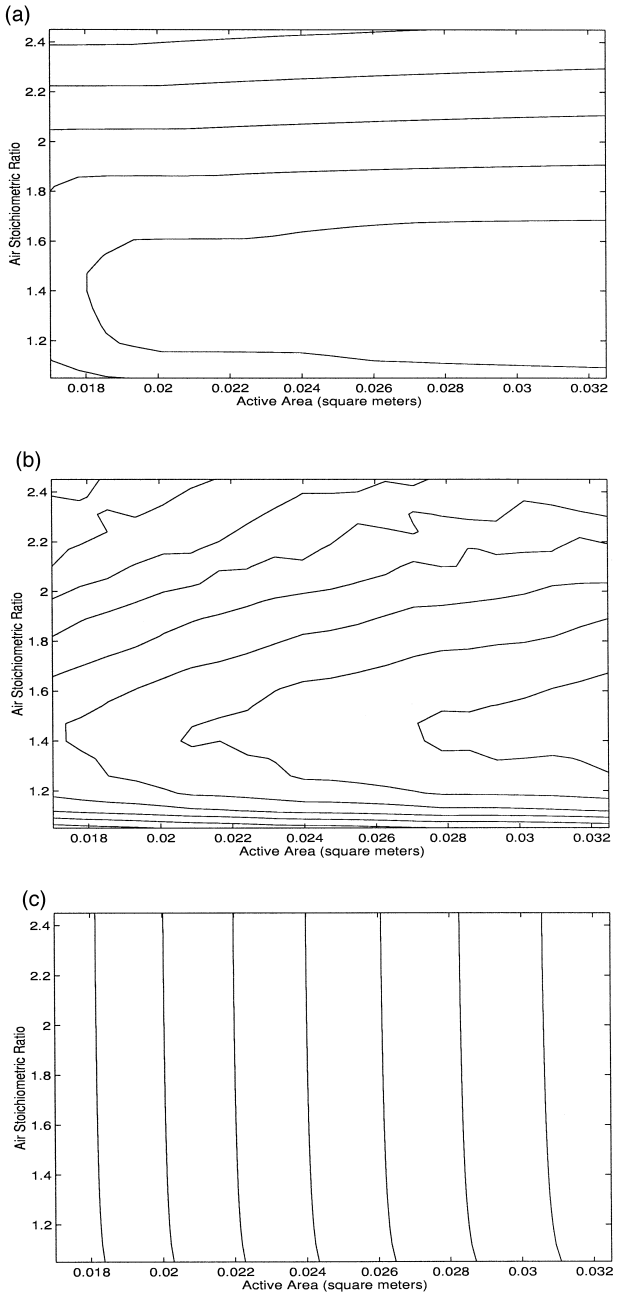

Fig. 8. Evaluation measures regarding both active area and air stoichiometric ratio. (a) Contour map of maximum net system power. (b) Contour map of USABC DST efficiency. (c) Contour map of system cost.

ratio and a steady increase of production costs with the increase of the air stoichiometric ratio.

Subsequently, the two design variables are considered simultaneously to obtain the 2-D contour maps of the three selected performance and cost evaluation measures as shown in Fig. 8.

4.3. Identification of the optimal design

The optimal design is carried out following the balanced design principle and identified through the joint optimization of system functional performance and production costs, using Eq. (4).

The functional performance and production cost indices are obtained using the fuel cell system performance and cost models discussed previously. The projected average performance and cost values are used as references to obtain the generally comparable dimensionless life-cycle

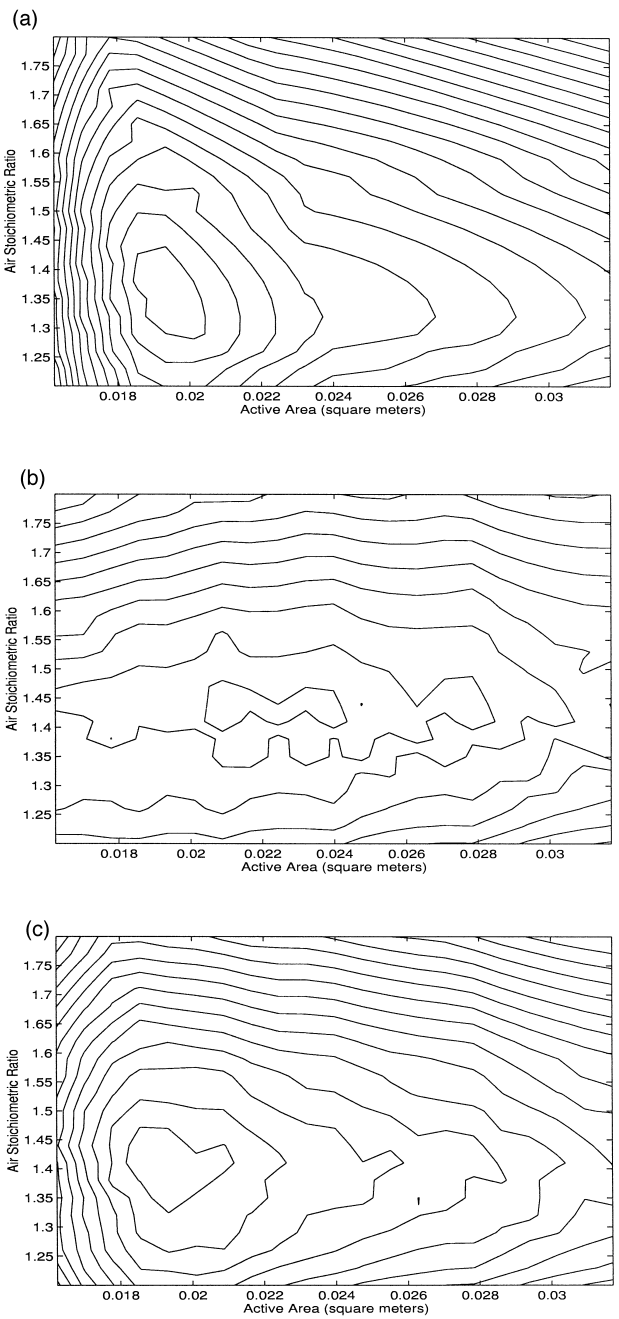

Fig. 9. Design quality indices considering two design parameters. (a) Maximum net system power and production costs (combined). (b) USABC DST efficiency and production costs (combined). (c) Maximum net system power, USABC DST efficiency and production costs (combined).

performance readings. In this case, the targeted area of the design variables, V, is selected as:

$$V = \{A_a, \chi | 1.624 \times 10^{-2}\ m^2 \le A_a \le 3.17 \times 10^{-2}\ m^2, 1.2 \le \chi \le 1.8\} \quad (40)$$

This approach is equivalent to a design improvement test, in which a given design is used as the reference, and the new design that leads to the maximum performance increase and minimum cost jump (or maximum cost reduction) is to be identified. The joint optimization automatically carry out the search and identify the optimum design solution once the reference is given.

The results of the joint optimization can be illustrated using a number of contour maps of the performance and cost indices with respect to the two design variables. These contour maps include (a) W_{net}^{max} and C, (b) η_{ave} and C, and (c) W_{net}^{max}, η_{ave}, and C, as illustrated in Fig. 9(a), (b), and (c), respectively. If we jointly consider the maximum net system power, USABC DST efficiency, and the production costs of the system, the optimal design is then at the active area of 0.0195 m^2 and air stoichiometric ratio at 1.4, as illustrated by Fig. 9(c). Similarly, if only one performance aspect is jointly considered with production costs, the optimal design can be found from Fig. 9(a) and (b).

5. Summary

In this work, the optimization-based, integrated concurrent design method was applied to the modeling, analysis and design of a general mechanical system—the transportation fuel cell system. A general optimal design model considering all product life-cycle performance aspects was first introduced. Discussion was then focused on a simplified optimal design model, considering the two most important aspects of a product: functional performance and production costs. Issues involved in the joint optimization of functional performance and production costs were addressed. These included the mathematical modeling of functional performance and production costs, the selection of design variables, and the conversion of performance and cost readings into a generally comparable, dimensionless measure. The approach used either an existing or an average design as the reference to seek the optimal design that leads to the maximum performance increase and minimum cost jump. The search was carried out automatically through the joint optimization.

To demonstrate this new approach, functional performance and production cost models of the Ballard Mark V fuel cell system were discussed. The joint optimization concurrently considers the maximum net system power, the USABC DST efficiency, and the production costs of the system with respect to two key design variables: the active area and the air stoichiometric ratio in searching the optimal design solution.

This approach breaks the traditional barrier between design (concerning functional performance) and manufacturing (concerning production costs), allowing both functional performance and production costs to be fed into early design phase and to be jointly optimized. The work is a continuation of the authors' earlier research on integrated concurrent engineering design.

6. List of symbols

A_a	active intersection area of fuel cell stacks (cm^2)
A_t	total intersection area of fuel cell stacks (cm^2)
C	total fuel cell system cost ($)
C_{air}	cost of air supply module ($)
C_{cell}	cost of a fuel cell ($)
C_{cont}	cost of control module ($)
C_{cool}	cost of cooling module ($)
C_{H_2}	cost of hydrogen supply module ($)
C_{hum}	cost of a humidification cell ($)
C_{stacks}	cost of stack module ($)
C_{stk_a}	cost of stack assembly ($)
C_{stk_m}	cost of stack material ($)
C_{O_2}*	concentration of oxygen (mol/cm^3)
E	open circuit voltage of a fuel cell (V)
F	Faraday's constant (96,487 C/equivalent)
f_{air}	air supply flow rate (m^3/s)
f_{H_2}	hydrogen supply flow rate (m^3/s)
I	current (A)
i	current density (A/cm^2)
n	number of equivalents involved in reaction
n_{cell}	number of cells in a stack (35)f
n_{H_2}	electron number per hydrogen molecule (2)
n_{hum}	number of humidification cells
n_{stack}	number of stacks in the system (24)
P_{air}	pressure of air (atm)
P_{H_2}	pressure of hydrogen (atm)
p_{H_2}*	effective partial pressure of hydrogen at gas/liquid interface (atm)
$p_{H_2O}^{sat}$	saturation pressure of water (atm)
p_{O_2}*	effective partial pressure of oxygen at gas/liquid interface (atm)
R	gas constant (8.3143 J/mol K)
T_c	temperature (°C)
T_k	temperature (K)
VSTP	specific molar volume of gas (22.4×10^{-3} m^3/mol)
V_{cell}	output voltage of a cell (V)
W_{ac}	power consumed by the air compressor (W)
W_{cool}	power consumed by cooling module including radiator fan and water pump (W)
W_{net}	net system power output (W)
W_{net}^{max}	maximum net system power output (W)
W_{sys}	system power output (W)
$x_{H_2O}^{anode}$	mole fraction of water at anode

$x_{H_2O}^{cathode}$	mole fraction of water at cathode
η	efficiency of the fuel cell system
η_{act}	voltage loss due to activation (V)
η_{ave}	USABC DST average efficiency
η_{ohmic}	voltage loss due to ohmic resistance (V)
χ	stoichiometric ratio of air
χ_{O_2}	fraction of oxygen in the air (0.21)

Acknowledgements

Financial support from the Natural Science and Engineering Research Council (NSERC) of Canada, British Gas Technology, and Ballard Power Systems through the Next Generation Fuel Cells for Transportation (NGFT) research program, and the technical assistance from Ballard Power Systems are gratefully acknowledged.

References

[1] L.J.M.J. Blomen, M.N. Mugerwa (Eds.), Fuel Cell Systems, Plenum, 1993.
[2] I. Stann, Fuel Cells—Realising the potential, Power Engineering Journal, April Issue (1993) 94–96.
[3] D. Xue, Z. Dong, Feature modeling incorporating tolerance and production process for concurrent design, Concurrent Engineering: Research and Applications 1 (1993) 107–116.
[4] D. Xue, Z. Dong, Developing a quantitative intelligent system for implementing concurrent engineering design, Journal of Intelligent Manufacturing 5 (1994) 251–267.
[5] D. Xue, J.H. Rousseau, Z. Dong, Joint optimization of performance and costs in integrated concurrent design: tolerance synthesis part, Engineering Design and Automation 2 (1) (1996) 73–89.
[6] B. Prasad, Concurrent Engineering Fundamentals, Vol. 1, Prentice Hall, 1996.
[7] P. O'Grady, R.E. Young, Issues in concurrent engineering systems, Journal of Design and Manufacturing 1 (1991) 27–34.
[8] A. Rosenblatt, G.F. Watson, Concurrent engineering, IEEE Spectrum 28 (7) (1991) 22–37.
[9] J.C. Amphlett, M. Farahani, R.F. Mann, B.A. Peppley, P.R. Roberge, The operation of a solid polymer fuel cell: a parametric model, Proceedings of the 26th Intersociety Energy Conversion Engineering Conference, 1991, pp. 624–629.
[10] J.C. Amphlett, R.M. Baumert, R.F. Mann, B.A. Peppley, P.R. Roberge, A. Rodrigues, Parametric modeling of the performance of a 5-kW proton-exchange membrane fuel cell stack, Journal of Power Sources 49 (1994) 349–356.
[11] J.C. Amphlett, R.M. Baumert, R.F. Mann, B.A. Peppley, P.R. Roberge, T.J. Harris, Performance modeling of the Ballard Mark IV solid polymer electrolyte fuel cell: I. Mechanistic model development, Journal of Electrochemical Society 142 (1) (1995) 1–8.
[12] J.C. Amphlett, R.M. Baumert, R.F. Mann, B.A. Peppley, P.R. Roberge, T.J. Harris, Performance modeling of the Ballard Mark IV solid polymer electrolyte fuel cell: II. Empirical model development, Journal of Electrochemical Society 142 (1) (1995) 9–15.
[13] R. Cownden, M. Nahon, Performance modeling and improvements of a solid polymer fuel cell system, Proceedings of the International Fuel Cell Conference, Kobe, Japan, 1996, pp. 355–358.
[14] J. Ronne, R. Podhorodeski, An integrated cost-performance model of a transportation solid polymer fuel cell system, Proceedings of the International Fuel Cell Conference, Kobe, Japan, 1996, pp. 385–388.
[15] T.E. Springer, T.A. Zawodzinski, S. Gottesfeld, Polymer electrolyte fuel cell model, Journal of Electrochemical Society 138 (8) (1991) 2334–2341.